Proceedings World Geothermal Congress 2020+1
Reykjavik, Iceland, April - October 2021

Simulation of Cryogenic Fracturing/Cooling around Boreholes with Liquid Nitrogen

Philip H. Winterfeld[1], Bowen Yao[1], Gabriel Amore[2], and Yu-Shu Wu[1]

[1]Petroleum Engineering Department, Colorado School of Mines, 1600 Arapahoe St., Golden, CO 80401, United States

[2]Newcrest Mining, Ltd., Level 8, 600 St. Kilda Road, Melbourne VIC 3004, Australia

Keywords: Simulation, cryogenic fracturing

ABSTRACT

During gold extraction from an open-pit mine, boreholes are drilled at the surface and packed with explosives that are detonated. Such a mine in a geothermally active zone can have a surface at an elevated temperature, which is detrimental to the integrity of the explosives that are packed in the boreholes. A proposed remedy for this is to cool the borehole with cryogenic fluid (liquid nitrogen) sufficiently such that explosives can be packed into them and operated safely.

We have been performing experimental studies of this cooling using concrete blocks to investigate rock behavior during cryogenic application, and numerical studies using a simulator of fluid and heat flow, and geomechanics in porous and fractured media. We modified our numerical simulator to handle fluid and heat flow for liquid nitrogen, as well as simulate fracture initiation and propagation resulting from cryogenic fluid injection.

We simulated two experiments, one a liquid nitrogen circulation in a concrete block and another with liquid nitrogen injection into a concrete block with an induced fracture, and matched measured temperature profiles well. We then ran two field-type simulations, one with injection wells in a five spot pattern that demonstrates cooling from liquid nitrogen injection, and another of liquid nitrogen injection into a well that demonstrates fracture initiation and propagation.

1. INTRODUCTION

During gold extraction from an open-pit mine, boreholes are drilled at the surface and packed with explosives that are detonated. The resulting blasted rock fragments are then transported away to be processed. An open-pit mine in a geothermally active zone can have a surface at an elevated temperature, which is detrimental to the integrity of the explosives that are packed in the boreholes. A proposed remedy for this is to inject cryogenic fluid (liquid nitrogen) into the boreholes in order to cool them sufficiently such that explosives can be packed into them and operated safely.

We have been performing both experimental and numerical studies of this cooling in order to determine the relationship between injected liquid nitrogen volume and ground cooling, and the duration of ground/borehole cooling after injection. The experimental studies have used concrete blocks (since actual rock samples have not been obtained as of this time) to investigate rock behavior during cryogenic application at the appropriate temperature and under a tri-axial confining stress field. Our numerical tool is a simulator of fluid and heat flow, and geomechanics in porous and fractured media that was modified to simulate fluid and heat flow of liquid nitrogen, as well as predict any potential fracture initiation and propagation resulting from liquid nitrogen injection into these boreholes.

Here, we describe some of the work we are doing regarding cryogenic fracturing/cooling around boreholes with liquid nitrogen, with emphasis on the numerical studies. We first describe the modifications to our simulator to handle liquid nitrogen transport and fracture initiation and propagation. Next, we simulate two experiments, one a liquid nitrogen circulation in a concrete block and another with liquid nitrogen injection into a concrete block with an induced fracture. Finally, we run two field-type simulations, one with injection wells in a five spot pattern that demonstrates cooling from liquid nitrogen injection, and another of liquid nitrogen injection into a well with fracture initiation and propagation.

2. SIMULATOR MODIFICATIONS

We modified our TOUGH2-CSM thermal-hydrological-mechanical simulator in this work. The TOUGH2-CSM fluid and heat flow formulation is based on the TOUGH2-MP formulation (Pruess et al., 1999) of mass and energy conservation equations that govern fluid and heat flow in general multiphase, multicomponent, multi-porosity systems. We previously added geomechanics to that formulation in two steps. In the first step (Winterfeld and Wu, 2014), we combined the equations governing stresses and displacements in elastic media to yield an equation for mean stress, which yielded a simplified geomechanical formulation. In the second step (Winterfeld and Wu, 2016), we extended that simplified geomechanical formulation to calculate the entire stress tensor efficiently. Additionally, porosity and permeability can depend on pressure and stress.

2.1 Physical Property Module

A component of the TOUGH2-CSM code is the fluid property module that calculates density, viscosity, enthalpy, and other properties. Examples of these modules are the TOUGH2 ones, such as EOS3 (Pruess et al., 1999), which calculates properties of water-air mixtures. We wrote such a module for nitrogen-water mixtures. Pure nitrogen and water data were obtained in tabular form as functions of pressure and temperature (Lemmon et al., 2020). We interpolate on these tables using a bilinear function. The temperature range for the data is from liquid nitrogen to an upper limit that would exceed temperatures encountered in the field, -210 °C to 350 °C, and a pressure upper limit of 3.0 MPa. There are two phases, a water phase and a nitrogen-rich one. The water phase

can be solid, liquid, or gas and the nitrogen-rich one can be liquid (composed of only nitrogen) or a gaseous mixture of nitrogen and water.

When nitrogen under flowing conditions boils, there is flow of two phases. This flow is turbulent and non-Darcy, so we approximate flow under these conditions as that of a lumped single phase. For Darcy flow of two phases, liquid (*l*) and gas (*g*), and one component (nitrogen), the equation for conservation of mass is:

$$\nabla \cdot \left[\frac{k k_{rg} \rho_g}{\mu_g} \nabla p_g + \frac{k k_{rl} \rho_l}{\mu_l} \nabla p_l \right] + \frac{\partial \left[\phi \left(s_g \rho_g + s_l \rho_l \right) \right]}{\partial t} = 0 \tag{1}$$

where k is absolute permeability, k_r is relative permeability, ρ is density, μ is viscosity, p is phase pressure, and ϕ is porosity. We neglect capillary pressure, assume relative permeability equals saturation, and define the lumped phase (*f*) density and viscosity as:

$$\rho_f = s_g \rho_g + s_l \rho_l \tag{2}$$

$$\frac{\rho_f}{\mu_f} = \frac{s_g \rho_g}{\mu_g} + \frac{s_l \rho_l}{\mu_l} \tag{3}$$

Then, Equation 1 assumes the form for a single phase:

$$\nabla \cdot \left[\frac{k \rho_f}{\mu_f} \nabla p \right] + \frac{\partial \left[\phi \rho_f \right]}{\partial t} = 0 \tag{4}$$

The equation for energy conservation for this flow is:

$$\nabla \cdot \left[\frac{k k_{rg} \rho_g h_g}{\mu_g} \nabla p_g + \frac{k k_{rl} \rho_l h_l}{\mu_l} \nabla p_l \right] + \frac{\partial \left[\phi \left(s_g \rho_g U_g + s_l \rho_l U_l \right) + \left(1 - \phi \right) \rho_r U_r \right]}{\partial t} = 0 \tag{5}$$

where h is specific enthalpy, U is specific internal energy, and subscript r refers to rock.. We again neglect capillary pressure and assume relative permeability equals saturation, and define the lumped phase specific internal energy and specific enthalpy as:

$$U_f = \frac{s_g \rho_g U_g + s_l \rho_l U_l}{s_g \rho_g + s_l \rho_l} \tag{6}$$

$$\frac{\rho_f h_f}{\mu_f} = \frac{s_g \rho_g h_g}{\mu_g} + \frac{s_l \rho_l h_l}{\mu_l} \tag{7}$$

Then, Equation 5 also assumes the form for a single phase:

$$\nabla \cdot \left[\frac{k \rho_f h_f}{\mu_f} \nabla p \right] + \frac{\partial \left[\phi \rho_f U_f + \left(1 - \phi \right) \rho_r U_r \right]}{\partial t} = 0 \tag{8}$$

Nitrogen properties change sharply during the transition between liquid to gas. For example, Figure 1 shows density versus temperature for 1 MPa pressure (solid line). Nitrogen boils at -169.4 °C and there is a discontinuity in density between the liquid value of 665.85 kg/m^3 and the gaseous value of 4.13 kg/m^3. We approximate this transition by "blurring" it over a few degrees above and below the boiling point, where nitrogen density changes continuously between the gaseous and liquid values, shown by the dashed line in Figure 1. The same is done for other tabular nitrogen properties, namely the enthalpy-density product and the density-viscosity ratio. These combinations, rather than enthalpy and viscosity alone, were chosen since they improve numerical performance.

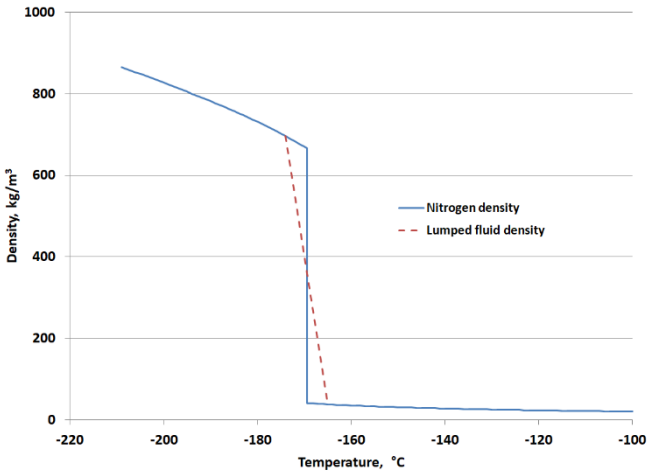

Figure 1. Nitrogen density versus temperature for 1 MPa pressure (solid line) with liquid-gas transition at -169.4 °C; lumped fluid density versus temperature (dashed line).

Finally, the final state of our experiments and simulations are not expected to be in the two-phase region for nitrogen, so the overall enthalpy changes will not be effected by this lumped fluid approximation.

2.2 Fracturing Model

Injection of liquid nitrogen into porous rock cools it, which is accompanied by induced thermal stresses that can result in cryogenic fracturing. We added a simple fracturing formulation to TOUGH2-CSM. In the field operation, liquid nitrogen is injected into a borehole through which it can enter the formation. This injection cools and pressurizes the borehole and fracturing is assumed to commence when the borehole fails. Schmidt and Zoback (1989) presented the following borehole failure criterion for an uncased hole, expressed as a breakdown pressure, p_b:

$$p_b = \frac{3\sigma_{\min} - \sigma_{\max} + \sigma_{tens} - \alpha p_{res}\dfrac{1-2\nu}{1-\nu}}{1+\delta-\alpha\dfrac{1-2\nu}{1-\nu}} \tag{9}$$

where $\sigma_{\min}$ is the minimum in-situ stress, $\sigma_{\max}$ is the maximum in-situ stress, σ_{tens} is the rock tensile strength, p_{res} is formation pressure, α is Biot's coefficient, ν is Poisson's ratio, and δ is a parameter. Equation 9 was derived from the state of stress around a borehole (Haimson and Fairhurst, 1967). We extend this analysis to include thermal stresses by superposing an approximation for the induced thermal stresses in the near-borehole region, given by (Timoshenko and Goodier, 1951):

$$\sigma_{therm} = \beta E\left(T - T_{ref}\right) \tag{10}$$

where T is temperature of the borehole, E is Young's modulus, β is linear thermal expansion coefficient, and T_{ref} is temperature for a thermally unstrained case:

$$p_b = \frac{3\sigma_{\min} - \sigma_{\max} + \sigma_{tens} + \sigma_{therm} - \alpha p_{res}\dfrac{1-2\nu}{1-\nu}}{1+\delta-\alpha\dfrac{1-2\nu}{1-\nu}} \tag{11}$$

After the borehole reaches the breakdown pressure, failure occurs and fractures can initiate and propagate in the formation. This is assumed to occur when the effective plus thermal stresses exceed the rock tensile stress:

$$\sigma_{tens} \le -\left(\sigma_{\min} - \alpha p\right) - \sigma_{therm} \tag{12}$$

In our finite-difference simulator, Equation 11 is the fracture initiation criterion that is applied to grid blocks containing the borehole and Equation 12 is the fracture initiation criterion that is applied to other grid blocks. When a fracture initiates in a grid block, the grid block porosity and permeability are modified to account for the presence of a fracture, which we correlate as the following functions:

$$\phi = \phi\left(T, T_{frac}\right) \tag{13}$$

$$k_l = k_l\left(\phi\right) \tag{14}$$

where T_{frac} is the fracture initiation temperature and subscript l refers to the permeability direction. The porosity function is constrained to be continuous at the fracture initiation temperature. The permeability modification is only applied to directions perpendicular to the minimum stress direction since an induced fracture would be perpendicular to that direction and the permeability in that direction would be relatively unchanged.

3. CRYOGENIC FRACTURING EXPERIMENT AND FIELD SIMULATIONS

Our cryogenic fracturing experiments were done on 8-inch concrete cubes made of Portland cement. A half-inch borehole was drilled into the top face of the cube at the center to a depth of five inches. A casing was inserted in the borehole that extended to three inches in depth and a quarter-inch outer diameter tubing was inserted inside the casing that extended to four inches in depth. Liquid nitrogen was injected via the tubing and could return via the annulus between the inner surface of the casing and the outer surface of the tubing, as well as enter the concrete through the bottom two inches of the borehole which had no casing. Five thermocouples were placed at four inches in depth at the following areal coordinates (in inches): (1,1), (2,2), (3,3), (4,6), and (4,7). A schematic of the concrete cube is shown in Figure 2 and a photograph in Figure 3. Thermocouples are identified by their number, which appears next to each one in Figure 2, right.

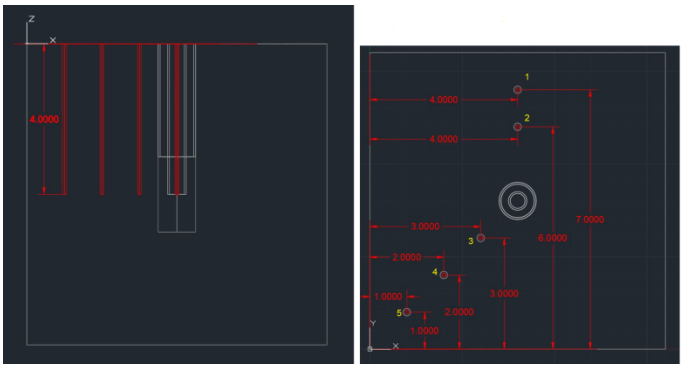

Figure 2. Side view (left) of concrete block showing thermocouple depth and borehole with tubing and casing. Top view (right) showing thermocouple locations (small circles) and numbering, and borehole at center.

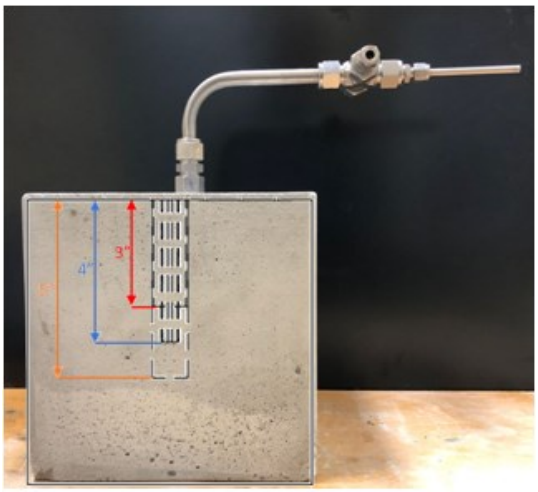

Figure 3. Concrete block with annulus/tubing assembly at top.

3.1 Experiment 14 Simulation

Experiment 14 was designed to test liquid nitrogen circulation in the experimental apparatus. In this experiment, the concrete block was heated to 100 °C in an oven and liquid nitrogen was injected through the tubing and produced through the annulus in the borehole for thirty minutes. Afterwards, nitrogen injection ceased and the concrete block equilibrated with the surroundings.

We simulated Experiment 14 on a 17×17×16 Cartesian grid with half-inch cubic grid blocks, except on the lateral surfaces of the grid where the dimension normal to the surface was halved, as shown in Figure 4. This was done in order for the thermocouple locations in Figure 2 to coincide with grid block centers.

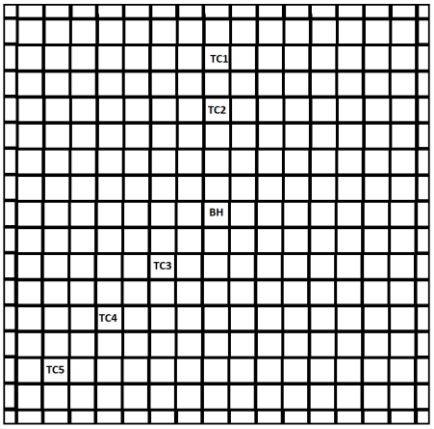

Figure 4. Top view of the simulation grid, with areal locations of the thermocouples (TH) and the borehole (BH).

The borehole and its contents were represented in detail by refining grid blocks that would contain the borehole volume, those situated at the areal center of the top (BH in Figure 4) and extending in depth to five inches (x- and y-direction index 9 and z-direction indices 1 through 10 in the Cartesian grid). This refinement is shown in Figure 5.

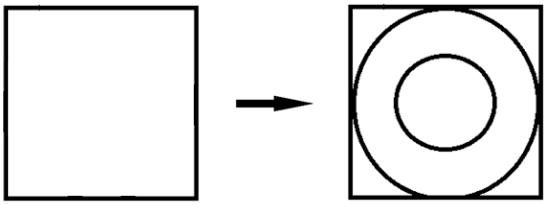

Figure 5. Top view of grid block refinement in borehole (BH) column.

The tubing is represented by the inner circle in Figure 5; the casing and the volume between the casing inner surface and the tubing outer surface is represented by the annulus outside of the inner circle; the region outside the annulus represents concrete. For depths below the end of the tubing or the casing, the volumes associated them would represent void. Figure 6 shows a cross section of the "BH" column of grid blocks.

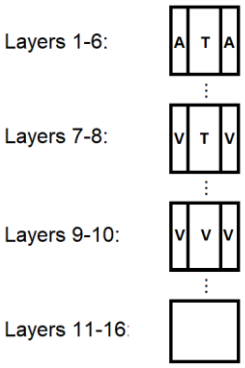

Figure 6. "BH" column of grid blocks, showing grid blocks containing tubing (T), annulus (A) that contains casing and volume between tubing and casing, and void (V). The bottom six grid blocks are concrete. The top ten layers also contain concrete, which is not shown.

The material properties of these regions, Concrete, Tubing, Annulus, and Void, are listed in Table 1. The Tubing and Annulus regions contain metal and empty space, so their porosity reflects the relative volumes of each. In addition, both regions only conduct fluid in the z-direction, so their permeabilities in the other directions are zero.

Table 1. Material region properties.

	Porosity	x,y-Perm., m^2	z-Perm., m^2	Thermal Cond., W/m-K	Heat Capacity, J/kg-K
Concrete	0.0956	10^{-15}	10^{-15}	1.8	828.0

Tubing	0.5476	0	10^{-10}	16.3	502.0
Annulus	0.6759	0	10^{-10}	16.3	502.0
Void	0.9900	10^{-10}	10^{-10}	1.8	828.0

Initially, the concrete block was at 100 °C, contained nitrogen gas, and the lateral surfaces of the block were constrained to be at ambient pressure so fluid could leave the system through them. Figure 7 shows a comparison of measured versus simulated temperatures, as well as cumulative nitrogen injected (a total of 7.6 kg). In the simulation, injection occurs in the Tubing grid block that lies in the top layer. The temperature there is reported in Figure 7 as BHT, and matches that of TC17 in the experiment. Before 1800 seconds, those temperatures are that for liquid nitrogen. The overall temperature trends from the thermocouples and from simulation are similar, with a minimum just below 50 °C and with a similar equilibration profile after injection has ceased. This simulation served as a verification of our model and its input data.

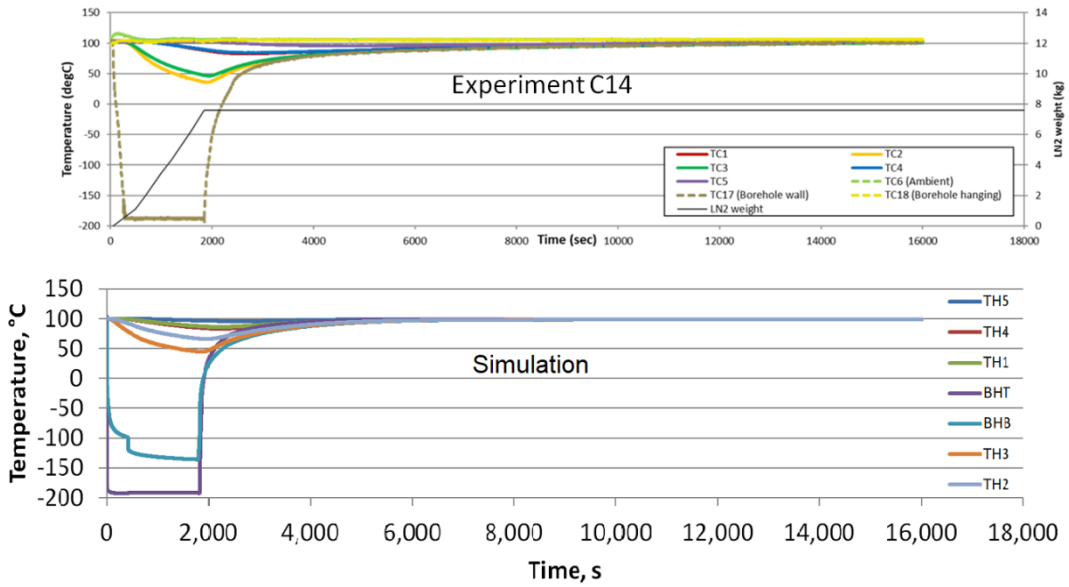

Figure 7. Comparision of Experiment 14 data, top, to simulation, bottom.

3.2 Experiment 19 Simulation

Experiment 19 was carried out with an induced fracture along the y-axis. The concrete block was heated to 200 °C in an oven and liquid nitrogen was injected through the tubing for 53 minutes. The annulus was closed so the nitrogen flowed through the concrete block, preferably through the fracture, to the surroundings. Afterwards, nitrogen injection ceased and the concrete block equilibrated with the surroundings.

We simulated Experiment 19 starting with the same grid and material properties as Experiment 14. We represented the fracture as an xz-plane of grid blocks that intersect the borehole and have a high permeability, as shown in Figure 8. The fracture communicates with the surroundings only through the top of the concrete block, which was also the case in the experiment.

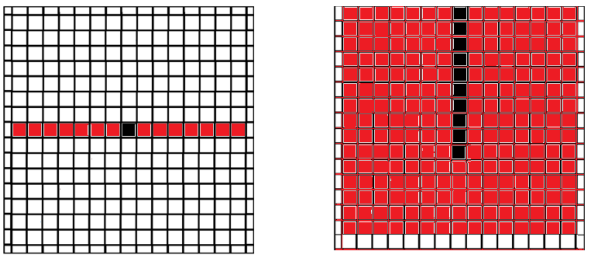

Figure 8. Top (left) and side (right) views of grid with high permeability grid blocks that represent fracture in red.

Initially, the concrete block was at 200 °C and contained nitrogen gas. A total of 8.35 kg of liquid nitrogen was injected. Figure 9 shows a comparison of measured versus simulated temperatures.

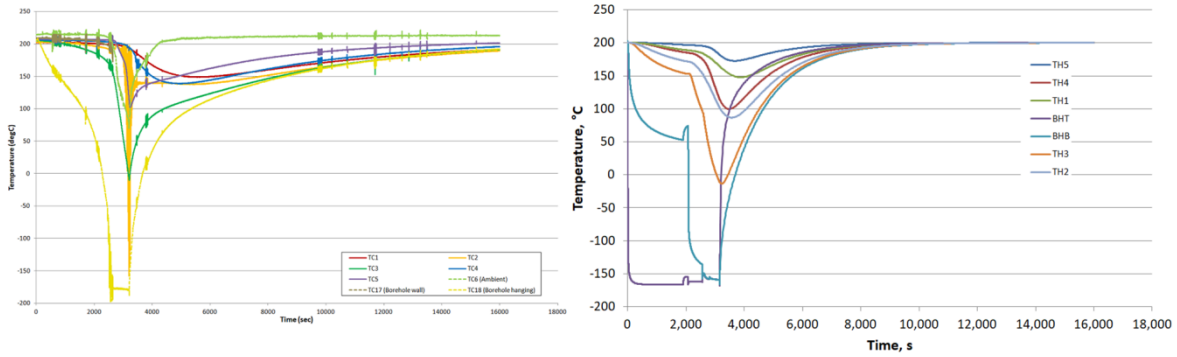

Figure 9. Comparision of Experiment 19 data, left, to simulation, right.

The minimum temperatures at the end of nitrogen injection for thermocouple TH3 and the simulation are similar, both slightly below 0 °C. The equilibration afterwards of the thermocouples and the simulation follow the same trend. The simulated temperature at the nitrogen injector site, BHT, is a bit higher than in the Experiment 14 simulation. One explanation is in the simulation, the injected nitrogen is transported away from the borehole quicker due to the presence of the fracture, so there is less cooling that region. In addition, the simulated fracture is an idealization of the actual fracture, which is irregular in shape.

3.3 Field Simulation I

We ran a simulation of a field-type case to determine the radius of cooling for a given amount of injected liquid nitrogen in a well configuration representative of those that would occur in the field. Rock density was 2300 kg/m^3, heat capacity was 828 J/kg-K, thermal conductivity was 4.0 W/m-K, porosity was 0.2, and permeability was 10^{-13} m^2. The simulation domain was 36×36×30 m and grid was 51×51×30, as shown in Figure 10.

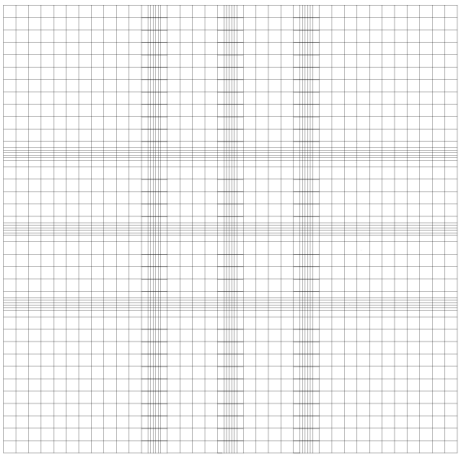

Figure 10. Areal view of grid for Field Simulation I.

Five injection wells were arranged in a 5-spot pattern, one at the center of Figure 10, and the other four at the center of the refined regions located diagonally from the center refined region. The wells were completed from 2 to 14 m depth. The initial temperature varied linearly with depth, 30 °C at 0 m depth and 177 °C at 30 m depth, nitrogen was initially present, and the lateral surfaces of the simulation domain were at ambient pressure so fluid could leave the system through them. Liquid nitrogen was injected into each well at 4.8 bbl/min for 6.33 hours and injection ceased for an additional twelve hours.

Figure 11 shows the xy-temperature profile for 8 m depth at the end of injection. The profile of the central well is symmetrical and those of the other wells reflect the pressurization of the central well that causes fluid to flow away from it.

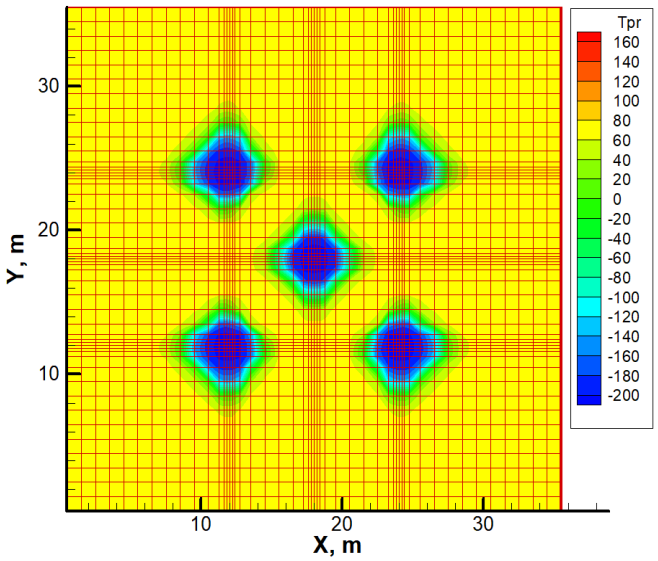

Figure 11. Temperature at 8 m depth, end of injection.

Figure 12 shows the surface temperature profile twelve hours after the end of injection. There is little change in temperature, indicating that cooling around the well will be maintained for times such as these. In addition, the radii of the cooled zones are 3.5 to 4.5 m.

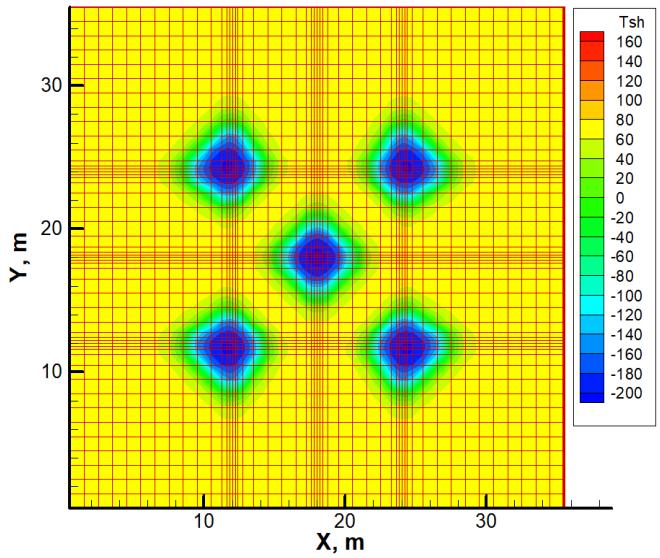

Figure 12. Temperature at 8 m depth, twelve hours after end of injection.

3.4 Field Simulation II

We ran a simulation of a field-type case to demonstrate the effect of cryogenic fracturing on borehole cooling from liquid nitrogen injection. The simulation domain was 30.5×30.5×20 m. Rock properties were the same as in the previous example, and additionally, tensile strength was 4.0 MPa, Young's modulus was 1.5 GPa, Poisson's ration was ν=0.33, and thermal expansion coefficient was $\beta=10^{-5}$ m^{-1}. The initial temperature varied linearly with depth, 30 °C at 0 m depth and 128 °C at 20 m depth, nitrogen was initially present, and the lateral surfaces of the simulation domain communicated with the surroundings. The initial stress tensor was in mechanical equilibrium and the minimum stress direction was the z-direction. There was one well at the areal center and completed from 2 to 14 m depth. Liquid nitrogen was injected into the well at 4.8 bbl/min for 6.33 hours and injection ceased for an additional twelve hours. The simulation grid was 61×61×40 (148,840 blocks) and grid blocks were 1/2 m cubes. Once a grid block fractured, either from reaching the breakdown pressure (Equation 11) or having its tensile strength exceeded (Equation 12), porosity varied linearly with temperature and permeability varied linearly with porosity:

$$\frac{\phi-\phi_0}{\phi_1-\phi_0}=\frac{T-T_0}{T_1-T_0} \tag{15}$$

$$\frac{k_l-k_{l,0}}{k_{l,1}-k_{l,0}}=\frac{\phi-\phi_0}{\phi_1-\phi_0} \tag{16}$$

Parameters for this variation are: T_I=-210 °C, T_0 is the temperature at which fracturing occurs, Φ_I=0.25, Φ_0=0.20, $k_{l,I}$=10^{-10}, and $k_{l,0}$=10^{-13}, l=x,y These conditions applied to all grid blocks and fractures originated at those containing the completed portion of the well at I=31, J=31, and K=5-28, where I, J, and K are x-, y-, and z-direction grid block index, respectively.

Figure 13 shows the yz-temperature profile through the well at the end of injection.

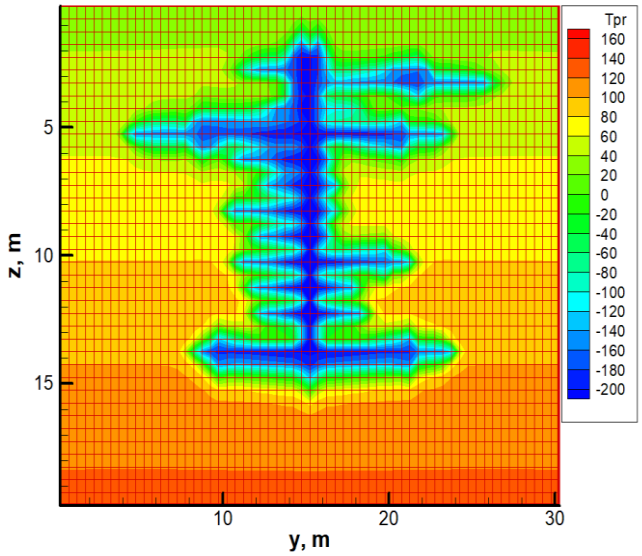

Figure 13. Temperature profile for yz-cross section through well at the end of injection.

All grid blocks containing completions have fractured by exceeding the breakdown pressure. Fractures then propagated in the xy-plane because the minimum stress direction is vertical. As fractures propagated, cold fluid flowed preferentially into them, which increased the permeability in the x- and y-directions and favored additional fracture propagation. This positive feedback resulted in preferred flow paths forming. Figure 13 shows two larger colder regions at the top and bottom of the completed interval. These regions have preferred flow paths due to the lower ambient temperature at the top of the completed interval and the higher pressure at the bottom, both of which lower the breakdown pressure. Finally, the colder regions exhibit irregularity in shape even though the simulation domain is axially symmetric around the injection well. The mass, energy and momentum (geomechanical) conservation equations are nonlinear and are solved using the iterative Newton-Raphson method. There is a convergence criterion for this method, which results in primary variables differing slightly from their "exact" values for each time step. Because simulations such as this require many time steps, thousands or even tens of thousands, and there is a positive feedback associated with the flow of cold fluid along a given direction, the numerical irregularities in the solution could be magnified to result in these irregular configurations.

Figure 14 shows the yz-temperature profile through the well twelve hours after the end of injection. There is significant warming of the colder regions that extend outward from the well. These regions are overlain and underlain by warmer ones, as shown in Figure 13, and heat is exchanged between them.

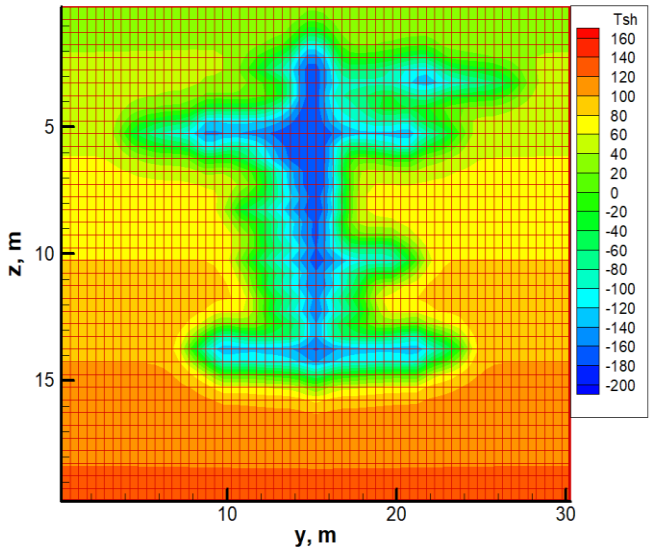

Figure 14. Temperature profile for yz-cross section through well twelve hours after the end of injection.

4. CONCLUSIONS

We modified our existing thermal-hydrological-mechanical simulator of fluid and heat flow, and geomechanics in porous and fractured media to additionally simulate cryogenic fracturing and cooling using liquid nitrogen.

We validated our modified simulator by matching experimental data, namely temperature profiles obtained from liquid nitrogen injection into cubic concrete samples. We then applied the simulator to field-type cases, and modeled cryogenic cooling in a five-spot well pattern and cooling around a single well with cryogenic fracturing. Our simulator gave information that would be useful for designing cryogenic cooling in the field.

ACKNOWLEDGEMENTS

This work was supported by EMG Research Center in Colorado School of Mines and Newcrest Mining Ltd.

REFERENCES

Lemmon, E. W., McLinden, M. O., and Friend, D. G., 2020. Thermophysical Properties of Fluid Systems in NIST Chemistry WebBook, NIST Standard Reference Database Number 69, Eds. P.J. Linstrom and W.G. Mallard, National Institute of Standards and Technology, Gaithersburg MD, 20899, https://doi.org/10.18434/T4D303.

Haimson, B. C. and Fairhurst, C., 1967. Initiation and extension of hydraulic fractures in rocks. *SPE Journal*, September, p. 310-318.

Pruess, K., C. Oldenburg, and G. Moridis. 1999. TOUGH2 User's Guide, Version 2.0. Report LBNL-43134, Lawrence Berkeley National Laboratory, Berkeley, California.

Schmidt, D. R. and Zoback, M. D., 1989. Breakdown equation employing a modified effective stress relation for tensile failure. *Int. J. Rock mech. Min. Sci. and Geomech. Abstr*. **26** (6) p. 499-506.

Timoshenko, S. and Goodier, J. N., 1951. Theory of elasticity, McGraw-Hill Book Company, Inc, New York.

Winterfeld P. H. and Wu Y.-S. 2014. Simulation of CO_2 Sequestration in Brine Aquifers with Geomechanical Coupling. In *Computational Models for CO_2 Sequestration and Compressed Air Energy Storage*, edited by J. Bundschuh and R. Al-Khoury, Chapter 8, pp. 275-303, New York, NY: CRC Press.

Winterfeld, P. H. and Y.-S. Wu. 2016. Simulation of Coupled Thermal/Hydrological/Mechanical Phenomena in Porous Media. *SPE Journal* **21** (3): 1041–49.